Atomic Layer Deposition Fabricating of Ceramic Nanofiltration Membranes for Efficient Separation of Dyes from Water

He Chen, Shanshan Wu, Xiaojuan Jia, Sen Xiong, and Yong Wang
State Key Laboratory of Materials-Oriented Chemical Engineering, College of Chemical Engineering, Nanjing Tech University, Nanjing 210009, P.R. China

DOI 10.1002/aic.16097
Published online January 31, 2018 in Wiley Online Library (wileyonlinelibrary.com)

To meet the strong need for highly efficient and controllable manufacturing methods to ceramic nanofiltration (NF) membranes, we use atomic layer deposition (ALD) to prepare NF membranes by tightening ultrafiltration (UF) membranes. We confine the ALD deposition of TiO_2 to the near-surface region of substrate UF membranes. The pores (~5 nm) in the selective layers are progressively reduced, thus transforming the original UF membranes to NF ones at acceptable expense of permeability. A molecular-weight-cut-off (MWCO) down to 890 Da is obtained after merely 40 cycles and the water permeability remains as high as 32 $L{\cdot}m^{-2}{\cdot}h^{-1}{\cdot}bar^{-1}$. MWCOs can be flexibly tuned by altering ALD cycles, which is lowered down to 410 Da with 60 ALD cycles. The deposited membranes are used to remove dyes from water and they show significantly enhanced rejection to negatively charged dyes. © 2018 American Institute of Chemical Engineers *AIChE J*, 64: 2670–2678, 2018

Keywords: atomic layer deposition, ceramic membranes, nanofiltration, dye removal

Introduction

Atomic layer deposition (ALD) is a technique for depositing highly conformal and uniform thin films on substrates by exposing their surfaces to alternate gaseous precursors.[1–5] In the past two decades, the applications of ALD have been extended from the traditional field of microelectronics to the synthesis of functional materials.[6,7] In contrast to chemical vapor deposition in which precursors are present simultaneously in the deposition chamber, precursors are introduced into the chamber as a series of non-overlapping, sequential pulses during ALD processes. In each of these pulses the precursors react with the substrate in a self-limiting way, so that the reaction terminates once all the reactive sites on the substrate surface are consumed up. As a result, the maximum amount of material deposited on the surface after an ALD cycle is determined by the nature of the reactions between precursors and substrate surface and between the two precursors. Therefore, ALD is particularly suitable for the precise modification and functionalization of nanoporous materials. A number of materials including oxides, metals, sulfides and even polymers[8,9] have been deposited on various substrates including ceramics,[10–12] polymers,[13–19] carbon materials,[20,21] or biomolecules.[22,23] Moreover, there are a few reports on using ALD to modify/functionalize porous separation membranes which are also a typical type of nanoporous materials.[24–33] Previously, these works were exclusively focused on the reduction of membranes pores for gas separation. Starting from the year of 2011, we extended the ALD method to the modification and functionalization of UF[11,12,19,34–41] and microfiltration (MF)[42–45] membranes for the applications of water treatment. In these studies, the purposes include (1) to tune the pore size of porous polymeric membranes with subangstrom preciseness to fit various separation systems, and (2) to enhance the surface hydrophilicity and fouling resistance, which is essential in water treatment.

Our previous works have proved that ALD could also be used in the modification of inorganic ceramic membranes to upgrade separation performances.[11,12] The pore size and consequently the permeation of ceramic MF membranes were tuned simply by ALD deposition of Al_2O_3.[11] By increasing the deposition cycle numbers, the water permeability was decreased whilst the retention was increased, and the original MF membranes were finally tightened to UF membranes. However, simply repeating ALD cycles on the MF substrate membranes did not lead to NF membranes. One reason is that thousands of deposition cycles would be required to reach a desirable rejection in the NF category, which is very tedious and time-consuming. The other one is that most of the pores in the original MF membranes had been completely sealed after heavy deposition, leading to a great loss in permeability. Because of the wide pore size distribution of the UF substrate membranes, there are still present of abnormally large pores in the deposited membranes, which prevents the realization of a rejection capability to the NF level because of the leaking effect of the remaining large pores.

Alternatively, we turned to another ALD-based strategy to produce ceramic NF membranes. We used tubular ceramic ultrafiltration (UF) membranes with a mean pore size of ~5 nm as the substrates.[12] Titanicone layers with varied thicknesses were ALD-deposited onto the surface of the membranes by replacing water with ethylene glycol as the oxidant

Correspondence concerning this article should be addressed to Y. Wang at yongwang@njtech.edu.cn

precursor. The deposited membranes were subsequently calcined to remove the organic moieties, producing microporous TiO_2 layers which deliver a NF separation property. The as-prepared ceramic NF membranes exhibited a MWCO of ~680 Da and water permeability of ~30 $L \cdot m^{-2} \cdot h^{-1} \cdot bar^{-1}$. Such a permselectivity is outstanding compared to the NF membranes prepared by the sol-gel method. In this strategy, the pore sizes and in consequence, the size-sieving properties are predominantly determined by the size of the organic moieties in the precursors and therefore, there is limited room to adjust the pore sizes by altering the deposition parameters. Moreover, this strategy contains two steps: deposition and calcination, and it also typically requires several hundreds of ALD cycles to form a dense metalcone layer covering the porous substrates, which are necessary for the formation of micropores fitting in the NF category by subsequent calcination. Several hundreds of ALD cycles mean considerable consumption of chemicals (precursors), time, and energy. Therefore, from the aspect of upscaling and large-scale manufacturing, this ALD strategy based on deposition of metalcone is still somewhat complicated and tedious and may suffer from low production efficiency. Therefore, there remains a strong desire for highly convenient and efficient methods to manufacturing ceramic NF membranes. Inspired by our previous work in which MF membranes can be progressively tuned to UF membranes simply by repeating ALD cycles, we anticipate that NF membranes can be manufactured by continuously depositing oxides on UF membranes, and the required ALD cycles would not be too many if the substrate membranes have small pores, for example, pore sizes less than 10 nm.

In the present work, tubular ceramic UF membranes with the mean pore size of ~5 nm are used as substrates. We deposit thin TiO_2 layers with varied thickness on the surface of the membranes by gradually enhancing the deposition cycle numbers. Short pulse durations and nonexposure mode are deliberately used to confine the deposition to take place predominantly in the near-surface region of the substrate UF membranes. Only a few tens of deposition cycles are required to tune the pore size since the pore size of the bare membranes is only ~5 nm, which is very time-saving and energy-efficient. Moreover, the deposited membranes exhibit adjustable NF performances with tunable MWCOs which can be achieved simply by changing the ALD cycle numbers. The deposited membranes are then explored to remove dyes with different molecular weights and charging properties from aqueous dye solutions, and they exhibit higher than 95% rejection to two negatively charged dyes with a molecular weight of ~1000 Da.

Experimental

Materials

Tubular ceramic UF membranes consisting of a TiO_2 inner separation layer and an α-alumina supporting layer (Fraunhofer-Institut für Keramische Technologien und Systeme IKTS, Germany) were used as substrates. The tubular membranes have an external diameter of 10 mm and a tube wall thickness of 1.7 mm, and the average pore size is ~ 5 nm according to the manufacturer. $TiCl_4$ (99.99%, Metalorganic Center, Nanjing University) and deionized water were served as metallic and oxygen source for the ALD process, respectively. N_2 with ultra-high purity of 99.999% (Tianhong Gas, Nanjing) was used as the purge and carrier gas during the ALD process. Silicon wafers (SY100W-01, Seyang Electronics) were cleaned with ethanol and deionized water, then dried in N_2 before using as control substrates.

Polyethylene glycol (PEG, Aladdin, Shanghai, China) with molecular weights of 600, 1500, 4000, and 10,000 Da were used to determine the MWCOs of the membranes. Methylene Blue (MB, 98.5%, Tianjin Chemical Reagent Research Institute, Tianjin, China), Cationic Yellow X-2RL (CYX, 98.5%, Tianjin Chemical Reagent Research Institute, Tianjin, China), Reactive Black 5 (RB5, 90%, Zhejiang Runtu Co., Ltd. Shangyu, China) and Rose Bengal (RB, 90%, J&K Chemicals, Shanghai, China) were used without further purification as model dyes with different molecular weights and charging properties. The properties and structures of the dyes are summarized in Table 1.

ALD of TiO_2

The membranes and monitoring silicon wafers were positioned in the chamber of the ALD reactor (Savannah S100, Cambridge NanoTech) and were heated at 100°C for 10 min before the deposition took place in vacuum (~1 Torr). The nonexposure mode was selected deliberately with the expectation that the reaction mainly takes place in the near-surface area. In this mode, no exposure time was included, and there would be no enough time for the precursors to enter into the deep interior of the membranes. Both $TiCl_4$ and water were maintained at room temperature. $TiCl_4$ and water vapor were pulsed into the reactor alternatively. For one TiO_2 ALD cycle, the $TiCl_4$ and H_2O were pulsed into the chamber for 0.03 s and 0.015 s, respectively, and subsequently the chamber was purged for 10 s with a steady N_2 flow rate of 20 sccm. The ALD deposition was repeated for 20, 30, 40, 50 and 60 cycles.

Characterizations

A field emission scanning electron microscope (FESEM, Hitachi S-4800) was used to reveal the surface and cross-sectional morphologies of the membrane samples with an operating voltage of 5 kV. A thin layer of Pd/Au alloy was sputtering-coated onto the surface of the samples before SEM observations to avoid electron charging. The thickness of the TiO_2 films deposited on silicon wafers was determined by a spectroscopic ellipsometer (Complete EASEM-2000U, J. A. Woollam) with an incidence angle of 70°. The pHs of dye solutions were measured using a conventional glass pH electrode (FB-5, Fisher Scientific Inc.) under the same concentrations.

Separation and permeation performance

A homemade apparatus (shown in Figure 1) was used to measure the water permeability and the retention of PEG or dyes at room temperature under the pressure of 5 bar. The PEG feed solution had a total concentration of 3 g/L (the concentration of each PEG was 0.75 g/L) while every feed solution of dyes had a concentration of 50 mg/L. The PEG and dye retention rates of the membranes were determined by measuring the PEG or dye concentrations at both feed and permeate side. 1 L solution was used in each retention test, and the membranes were tested successively according to the deposition cycles. The rejection rates were calculated by the Eq. 1:

$$R(\%) = \left(1 - C_p/C_f\right) \times 100 \quad (1)$$

where R is the PEG or dye retention rate of the membranes, C_p and C_f are the concentration of PEG or dye solutions in the

Table 1. Properties and Structures of Dyes Used in This Work

Dye	Chemical Structure	MW (g/mol)	Charge
Methylene Blue	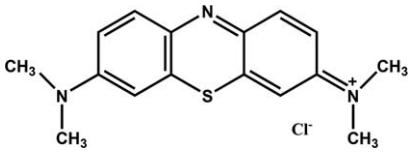	320	+
Cationic Yellow X-2RL	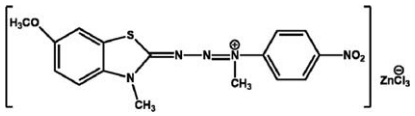	529.5	+
Reactive Black 5	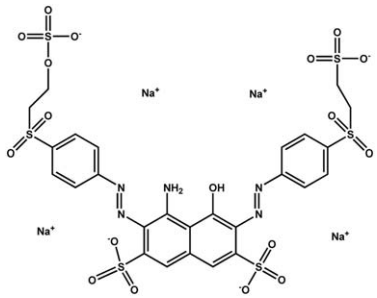	992	−
Rose Bengal	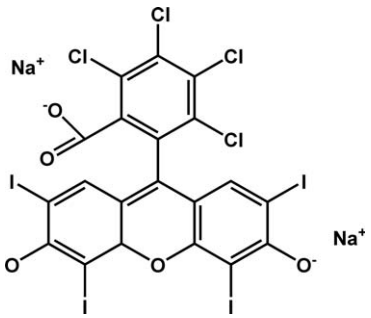	1017	−

permeate and feed solutions, respectively. Gel permeation chromatography (GPC, 1515, Waters, USA) was used to analyze the PEG solutions. The molecular weight of PEG which was 90% rejected was defined as the MWCO of the membranes. The dye concentrations were determined by absorption spectrometry using an UV–visible spectrophotometer (Nanodrop 1000, Thermo Fisher) at 665 nm, 431 nm, 598 nm and 548 nm for MB, CYX, RB5 and RB, respectively.

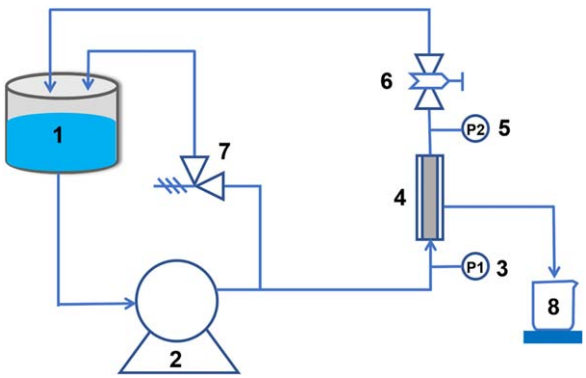

Figure 1. Schematic diagram of the filtration apparatus: (1) feed tank; (2) plunger pump; (3, 5) pressure gauge; (4) membrane module; (6) counterbalance valve; (7) safety valve and (8) beaker.

[Color figure can be viewed at wileyonlinelibrary.com]

Results and Discussion

The schematic of TiO_2 ALD on ceramic UF membranes was presented in Figure 2. The bare membrane possessed pores with a diameter of ~5 nm. The pore size decreased gradually with the increasing of deposition cycle numbers.

We first need to know the deposition behaviors under the set deposition conditions to make sure that the deposition takes place in the ALD mode and to know the growth rate of

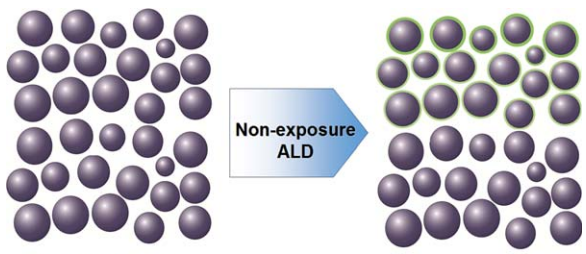

Figure 2. Schematic diagram of fabricating ceramic NF membranes from UF membranes using ALD in the nonexposure mode.

[Color figure can be viewed at wileyonlinelibrary.com]

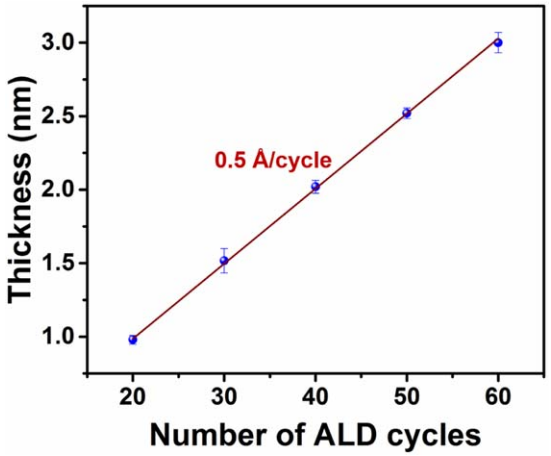

Figure 3. The thickness of TiO_2 layers deposited on silicon wafers with different cycle numbers.

[Color figure can be viewed at wileyonlinelibrary.com]

the TiO_2 layers. However, direct determination of the thickness of the deposited layers on the porous substrate membranes is difficult. Alternatively, we first investigated the deposition of TiO_2 on the smooth surface of silicon wafers under the set deposition conditions. Figure 3 presented the thickness of the TiO_2 layers produced with various cycles. There was a nearly perfectly linear increase of thickness with cycle numbers, implying that the deposition occurred truly in the ALD mode. The fitted growth rate was determined to be 0.5 Å/cycle, which is in good agreement with the results in literature utilizing the same precursors ($TiCl_4$ and H_2O).[46–48] The linear growth rate would be very beneficial for the precise modification of ceramic membranes to have predictable separation properties. Such a deposition behavior including the growth rate on silicon wafers was expected to be very close to that on porous membranes because the two substrates have similar surface chemistry (terminated by hydroxyl groups) and the deposition on membranes was confined to the near-surface region. Therefore, thus understood deposition behavior would be very helpful in our following studies on deposition on membrane substrates.

We then used SEM to reveal the morphology of the membranes after TiO_2 deposition with different ALD cycles. As can be seen from Figure 4a, the bare membrane had a porous structure composed of fused fine particulates. The gaps between the particulates defined the membrane pores with the diameter in the range of a few nanometers. It was clear from Figure 4 that the pore size of the membranes was continuously reduced with increasing ALD cycle numbers. Small pores remained discernable on the membrane surface when the cycle number was less than 60, and we can hardly observe any pores on the membrane with a cycle number of 60. Such an observation was, in general, consistent with the estimated pore sizes based on the growth rate of TiO_2. As the growth rate of TiO_2 was 0.5 Å/cycle under the used deposition conditions and the average pore size of the membrane was ~5 nm, we can estimate that the pore sizes are reduced to around 3, 2, 1 and 0 nm when the ALD cycles were 20, 30, 40 and 50, respectively. However, it should be noted that there may also exist some small pores on the membrane with 60 ALD cycles although they were under the detecting limit of SEM. The remaining pores were originated from big pores larger than the average 5-nm size in the original substrate membranes.

The evolution of the cross-sectional morphology of the membranes with TiO_2 deposition was further investigated. As shown in Figure 5a, the bare membrane exhibited a layered structure consisting of a thick supporting layer and a thin separation layer with a thickness of ~1.5 μm. After 20, 40 or 60 deposition cycles, no obvious changes could be seen in the supporting layer. It was worth noting that the deposition process also had quite weak influence on the cross-sectional morphology of the separation layer of the membranes as shown in Figures 5a–d. This should be ascribed to that a rather short pulse time (0.03 s and 0.015 s for $TiCl_4$ and H_2O, respectively) and nonexposure mode were used in this study, we did not expect the precursors diffuse into the selective layer, restricting the deposition process predominantly proceeding on the surface of the membranes. Therefore, the intact cross-sectional morphology after deposition confirmed that the deposition was predominantly taking places on the membrane surface. Such a deposition structure was essential to upgrade the selectivity at minimum expense of permeability loss as the interior in the

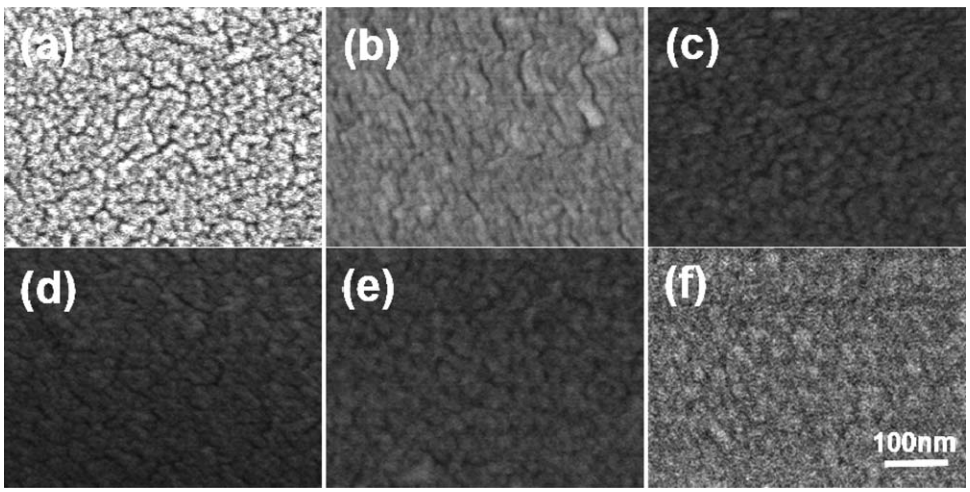

Figure 4. SEM images of the surface of (a) bare ceramic membrane, the TiO_2-deposited membrane with cycle numbers of (b) 20, (c) 30, (d) 40, (e) 50, and (f) 60.

(a)-(f) have the same magnification and the scale bar is shown in (f).

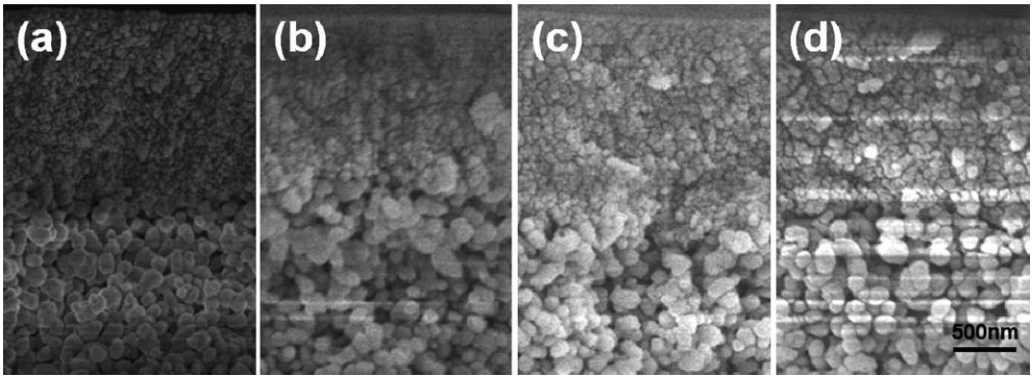

Figure 5. The cross-sectional SEM images of (a) the bare and the deposited membranes with (b) 20, (c) 40, and (d) 60 ALD cycles.

(a)–(d) have the same magnification and the scale bar is shown in (d).

selective layer largely remained its original porous state which would not lead to significantly increase the flow resistance.

The water permeability of the bare and deposited membranes was shown in Figure 6. The bare membrane exhibited a permeability of ~100 $L{\cdot}m^{-2}{\cdot}h^{-1}{\cdot}bar^{-1}$, which moderately dropped to ~75 $L{\cdot}m^{-2}{\cdot}h^{-1}{\cdot}bar^{-1}$ as a result of reduced pore size. The water permeability was further decreased to ~60 $L{\cdot}m^{-2}{\cdot}h^{-1}{\cdot}bar^{-1}$ and ~32 $L{\cdot}m^{-2}{\cdot}h^{-1}{\cdot}bar^{-1}$ after the membrane was deposited with 30 and 40 ALD cycles. With further extension of deposition cycles to 50 and 60, the permeability kept decreasing and reached ~18 and ~8 $L{\cdot}m^{-2}{\cdot}h^{-1}{\cdot}bar^{-1}$, respectively. Such relatively low permeabilities indicated that the pore sizes were significantly reduced on one side and the membranes were still water-permeable on the other although SEM imaging did not reveal any detectable pores on the surface of the membrane with 60 ALD cycles (Figure 3f).

The pore size of the selective layer dominates the separation performances of membranes. In the present work, the pore size was tuned simply by varying the deposition cycles. We investigated the retention performance of the deposited membranes by measuring their MWCOs using PEGs with different molecular weights as probe molecules. Figure 7a displayed the rejection rate of PEG as a function of molecular weight for the deposited membranes, and the corresponding MWCOs were presented in Figure 7b. The bare membrane exhibited a MWCO of ~7200 Da.[12] With 20 and 30 deposition cycles, the MWCO was significantly reduced to ~4400 Da and ~1800 Da, respectively, indicating the efficient pore size reduction effect of this near-surface deposition even after limited deposition cycles. Whilst the deposition cycles increased to 40, the MWCO was sharply tighten to ~890 Da, which steps into the range of NF. With further extending deposition cycles to 50 and 60, the MWCO was kept reducing and reached ~730 Da and ~410 Da, respectively. This should be ascribed to the progressive narrowing down of the pore sizes with continuous

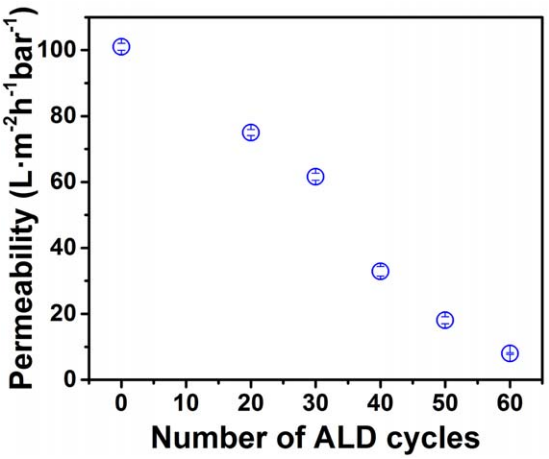

Figure 6. Water permeability of the bare membrane and the membranes with varied TiO_2 deposition cycles.

[Color figure can be viewed at wileyonlinelibrary.com]

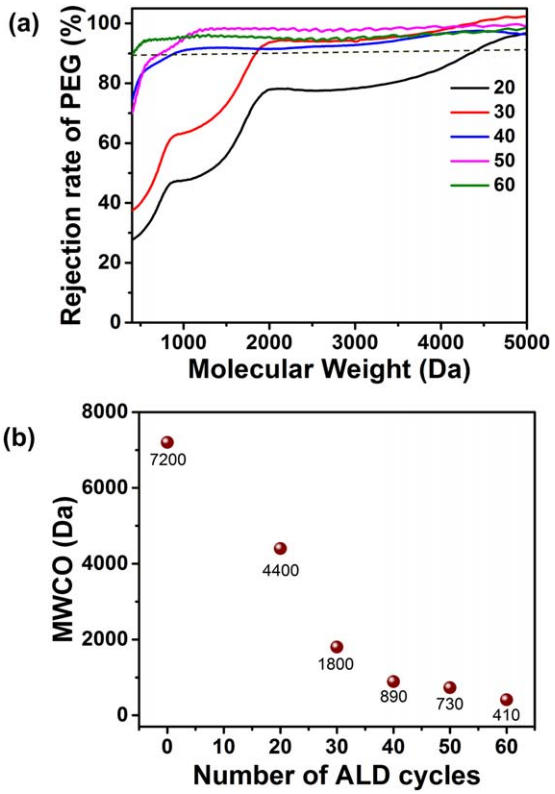

Figure 7. (a) PEG retention of the membranes with varied TiO_2 deposition cycles (the dashed line indicates the rejection of 90% at which the MWCO is determined), and (b) the corresponding MWCO versus cycles.

[Color figure can be viewed at wileyonlinelibrary.com]

Table 2. The Estimated Pore Size of Ceramic Membrane with Varied TiO_2 Deposition Cycles

Cycles	Estimated Pore Size (nm)
0	4.7
20	3.6
30	2.2
40	1.5
50	1.3
60	1.0

ALD deposition. That is, the size-sieving properties of the membranes can be flexibly tuned in a very convenient way by changing the ALD deposition cycles. The pore sizes of the membranes prepared by TiO_2 ALD deposition can be estimated by fitting their MWCOs into Eq. 2[49]:

$$r = 0.1673 \times (\mathrm{MW}\ (\mathrm{g/mol}))^{0.557} \quad (2)$$

The estimated pore sizes of the samples were presented in Table 2. As can be clearly seen, the pore sizes were decreased with increasing ALD cycles, and the reduction in pore sizes was slowed down when the deposition cycle number was 40 or more. This is because with increasing ALD cycles it would be more difficult for the precursors to react with the surface due to the steric hindrance, resulting in a lower deposition rate and consequently lower reduction in the effective pore size. Compared to other methods preparing ceramic NF membranes,[50–56] the ALD route developed in the current work is distinguished for its flexibility in progressively and precisely tuning the pore sizes and consequently the size-sieving properties of the membranes.

We then investigated the separation performances of the deposited membranes to aqueous solutions of four dyes with changing molecular weights and charging properties (the concentration of the feed solutions for all the four dyes was set to 50 $mg \cdot L^{-1}$) and the rejection rates were listed in Table 3. Two of the four dyes are negatively charged while the other two are positively charged, and their molecular weights vary in the range of ~300–1000 Da, allowing us to study the effect of surface charging and molecular sizes on the NF performances. The corresponding UV-vis spectra of the permeate, retentate, and feed of the dye solutions for the membranes with various ALD cycles numbers were given in Figures 8a–d, respectively. The bare membrane before ALD deposition exhibited weak retentions to all the four dyes. This is reasonable because they possessed a relatively large pore size of around 5 nm and their MWCO was around 7200 which was much larger than the molecular weights of all the four dyes. In addition, we noticed that the bare membranes displayed better retentions to RB5 and RB than to MB and CYX. This should be attributed to two factors: bigger molecular weights and different surface charging. Both RB5 and RB have a molecular weight of ~1000 Da, which should have a higher chance to be rejected by the membranes because of the mechanism of size sieving than MB and CYX which have a molecular weight of around or less than 500 Da. The other factor was the electrostatic interaction between the membrane and dye molecules. Since TiO_2 has an isoelectric point of 6.0,[55] the membrane with a TiO_2 depositing layer is negatively charged when they are exposed to aqueous dye solutions, all of which exhibit pH value of ~8. Therefore, there was an additional rejection mechanism of electrostatic repulsion between the membrane and the negatively charged RB5 and RB. Consequently, the bare membranes showed much lower retentions to positively charged dyes (MB and CYX) with lower molecular weights.

As shown in Table 3, after deposition the membranes showed remarkably enhanced retentions to all the four dyes, and the retention rates were increased with rising ALD cycles. Because deposition of TiO_2 on TiO_2 membranes does not change the surface charging properties of the membranes, the enhancement in retention are predominantly the result of the reduced pore sizes of the deposited membranes which had continuously reduced pore sizes with increasing ALD cycles. For MB and CYX, because their molecular weights are too small compared to the MWCO of the deposited membranes, their retention rate could be limitedly improved to 47.3% and 62.7% after deposition for 30 and 50 ALD cycles, respectively. Membranes with higher cycles did not allow a measurable permeability even under the pressure of 1.5 MPa. This was due to the pore clogging as a result of severe adsorption of dyes molecules on the pore walls. The two dyes are positively charged and they have strong electrostatic attraction to the negatively charged pore walls. The inner and outer surface of the membranes became darkly colored after filtration of the two dyes, which vividly indicated the severe adsorption of the two dyes in the membranes. Moreover, from Table 3 we can see that the membranes with different ALD cycles always exhibited higher retention rates to MB than CYX. Since the two dyes have similar molecular weight if we do not consider the part of their counter ions, the higher retention to MB can be attributed to the stronger clogging effect of MB to the membrane pores than CYX which was due to the more rigid and bulky organic moieties containing multiple rings in the molecules of MB. As can be seen clearly from Figure 8, the concentrations of retentates were even smaller than that of the feeds in the case of both MB and CYX, further evidencing that severe adsorption did occur during the filtration of positively charged dyes.

For the negatively charged dyes, the deposited membranes exhibited remarkably increased retentions. For instance, a cycle number of 20 was able to increase the retention of RB5 to 86.1% from 33.4% for the bare membrane, and a cycle number of 30 led to a retention rate of 96.2%. The retention rates were kept nearly unchanged with further increased cycle numbers. The much higher retention rates of the deposited membranes to negatively charged dyes than to positively charged dyes were due to the electrostatic repulsion between the pore walls and the negatively charged dyes and bigger molecular sizes of the negatively charged dyes. Moreover, we observed that the deposited membranes showed weaker retention to RB than to RB5. For example, to achieve a retention rate higher than 90% for RB5, the membrane was required to

Table 3. The Specific Rejection Rate of Different Dyes for the Bare and Deposited Membranes

	Rejection Rate of Different Dyes (%)			
Cycles	MB	CYX	RB5	RB
0	16.9	6.1	33.4	27.3
20	29.5	28.5	86.1	60.5
30	47.3	38.4	96.2	64.4
40	/	41.9	97.2	93.4
50	/	62.7	97.5	92.8
60	/	/	96.2	95.8

"/" stands for that no Solution would Permeate through the Membrane under 1.5 MPa for 10 min.

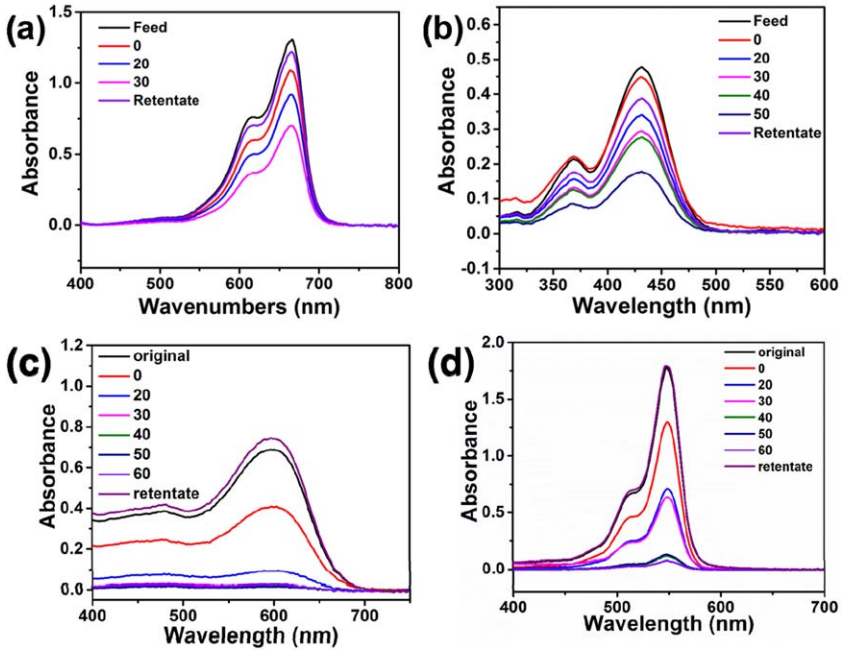

Figure 8. The UV-vis spectra of the feed, permeate, and retentate of (a) MB, (b) CYX, (c) RB5, and (d) RB aqueous solutions filtrated through the bare and deposited membranes with varied ALD cycles.

[Color figure can be viewed at wileyonlinelibrary.com]

be deposited for 30 ALD cycles. However, 40 ALD cycles were necessary for the membrane to achieve a retention rate of >90% to RB. The two negatively charged dyes have very close molecular weights and they both carry one single negative charge in each of their molecules when dissolved in water. Therefore, the difference in retention should be originated from the differences in their chemical structures, which has been frequently observed in other works of membrane separation of dye solutions.[57] RB5 possesses a relatively longer molecular chain than that of RB, resulting in larger steric hindrance than RB. Consequently, some of the RB5 molecules cannot pass through the pores vertically, which led to a higher rejection. As clearly shown in Figures 8c, d, for the two negatively charged dyes, the concentrations of the retentates were larger than that of the feeds, indicating that the adsorption was much less pronounced during filtration compared to the case of positively charged dyes. Moreover, Figures 8c, d also showed that membranes with larger ALD cycles always generated permeates with weaker characteristic peaks, confirming their stronger retention capabilities.

Conclusions

In this work, we demonstrated a facile and effective method to manufacture ceramic tubular NF membranes with tunable size-sieving properties. TiO_2 was ALD-deposited on ceramic UF membranes with a pore size of ~5 nm using $TiCl_4$ and H_2O as precursors. By controlling the pulse durations of the precursors, the deposition was limited to take place mainly in the near surface region in the selective layer of the UF substrate membranes. Due to the constant growth rate of TiO_2 ALD at 0.5 Å/cycle, the pore size of the membrane was precisely tuned by varying the deposition cycle numbers. The membrane was significantly tightened to have a MWCO of ~890 Da after merely 40 ALD cycles while its water permeability remained at a relatively high level of ~32 $L{\cdot}m^{-2}{\cdot}h^{-1}{\cdot}bar^{-1}$. Moreover, the separation properties of the membrane can be precisely tuned by varying the deposition cycle numbers. For instance, by increasing cycle numbers to 50 and 60, the MWCO of the membrane was reduced to ~730 Da and ~410 Da, respectively. The deposited membranes were further applied in rejection of dyes with different molecular weights and charges. The positively charged dyes tended to block the pores of the membranes due to severe adsorption, while the negatively charged dyes can be effectively rejected because of the narrowed pore size and the electrostatic repulsion. The membrane with 40 ALD cycles exhibited a rejection rates higher than 93% for the negatively charged dyes with the molecular weight of ~1000 Da. Considering that ALD is a versatile tool to deposit many different types of oxides, metals, and even polymers on substrate membranes, we expect that this method can be extended to prepare NF membranes with different material nature, for example, ZrO_2, to enhance the performances or to endow additional functionality to the membranes. We think that this strategy of controlling the ALD deposition in the near-surface regions in the selective layers would be applicable in the manufacturing of other membranes, thus to tighten the selectivity at minimum expense of permeation loss. Moreover, although ALD was originally used in microelectronics. However, the emergence of new ALD operations, for example, the customer-made large chambers,[58] and the roll-to-roll process,[59] reveals the great possibility for the continuous production of membranes in large scale.

Acknowledgments

Financial support from the National Basic Research Program of China (2015CB655301), the Natural Science Research Program of the Jiangsu Higher Education Institutions (13KJA430005), the Natural Science Foundation of Jiangsu Province (BK20150063), the Program of Excellent Innovation Teams of Jiangsu Higher Education Institutions, and the Project of Priority Academic Program Development of Jiangsu Higher Education Institutions (PAPD) is gratefully acknowledged.

Literature Cited

1. Puurunen RL. Surface chemistry of atomic layer deposition: a case study for the trimethylaluminum/water process. *J Appl Phys*. 2005; 97(12):121301
2. George SM. Atomic layer deposition: an overview. *Chem Rev*. 2010; 110(1):111–131.
3. George SM, Yoon B, Dameron AA. Surface chemistry for molecular layer deposition of organic and hybrid organic-inorganic polymers. *Acc Chem Res*. 2009;42(4):498–508.
4. Grigoras K, Airaksinen V-M, Franssila S. Coating of nanoporous membranes: atomic layer deposition versus sputtering. *J Nanosci Nanotechnol*. 2009;9(6):3763–3770.
5. Ritala M. Advanced ALE processes of amorphous and polycrystalline films. *Appl Surf Sci*. 1997;112:223–230.
6. Biercuk M, Monsma D, Marcus C, Becker J, Gordon R. Low-temperature atomic-layer-deposition lift-off method for microelectronic and nanoelectronic applications. *Appl Phys Lett*. 2003;83(12):2405–2407.
7. Knez M, Nielsch K, Niinistö L. Synthesis and surface engineering of complex nanostructures by atomic layer deposition. *Adv Mater*. 2007;19(21):3425–3438.
8. Putkonen M, Harjuoja J, Sajavaara T, Niinistö L. Atomic layer deposition of polyimide thin films. *J Mater Chem*. 2007;17(7):664–669.
9. Adamczyk NM, Dameron A, George S. Molecular layer deposition of poly (*p*-phenylene terephthalamide) films using terephthaloyl chloride and *p*-phenylenediamine. *Langmuir*. 2008;24(5):2081–2089.
10. Qin Y, Lee S-M, Pan A, Gösele U, Knez M. Rayleigh-instability-induced metal nanoparticle chains encapsulated in nanotubes produced by atomic layer deposition. *Nano Lett*. 2008;8(1):114–118.
11. Li F, Yang Y, Fan Y, Xing W, Wang Y. Modification of ceramic membranes for pore structure tailoring: the atomic layer deposition route. *J Membr Sci*. 2012;397–398:17–23.
12. Chen H, Jia X, Wei M, Wang Y. Ceramic tubular nanofiltration membranes with tunable performances by atomic layer deposition and calcination. *J Membr Sci*. 2017;528:95–102.
13. Kemell M, Färm E, Ritala M, Leskelä M. Surface modification of thermoplastics by atomic layer deposition of Al_2O_3 and TiO_2 thin films. *Eur Polym J*. 2008;44(11):3564–3570.
14. Liang X, George SM, Weimer AW, Li NH, Blackson JH, Harris JD, Li P. Synthesis of a novel porous polymer/ceramic composite material by low-temperature atomic layer deposition. *Chem Mater*. 2007; 19(22):5388–5394.
15. Liang X, King DM, Groner MD, Blackson JH, Harris JD, George SM, Weimer AW. Barrier properties of polymer/alumina nanocomposite membranes fabricated by atomic layer deposition. *J Membr Sci*. 2008;322(1):105–112.
16. Ras RH, Kemell M, de Wit J, Ritala M, ten Brinke G, Leskelä M, Ikkala O. Hollow inorganic nanospheres and nanotubes with tunable wall thicknesses by atomic layer deposition on self-assembled polymeric templates. *Adv Mater*. 2007;19(1):102–106.
17. Wang Y, Qin Y, Berger A, Yau E, He C, Zhang L, Gösele U, Knez M, Steinhart M. Nanoscopic morphologies in block copolymer nanorods as templates for atomic-layer deposition of semiconductors. *Adv Mater*. 2009;21(27):2763–2766.
18. Peng Q, Tseng YC, Darling SB, Elam JW. Nanoscopic patterned materials with tunable dimensions via atomic layer deposition on block copolymers. *Adv Mater*. 2010;22(45):5129–5133.
19. Sheng T, Chen H, Xiong S, Chen X, Wang Y. Atomic layer deposition of polyimide on microporous polyethersulfone membranes for enhanced and tunable performances. *AIChE J*. 2014;60(10):3614–3622.
20. Qin Y, Kim Y, Zhang L, Lee S-M, Yang RB, Pan ALian, Mathwig K, Alexe M, Gösele U, Knez M. Preparation and elastic properties of helical nanotubes obtained by atomic layer deposition with carbon nanocoils as templates. *Small*. 2010;6(8):910–914.
21. Wang X, Tabakman SM, Dai H. Atomic layer deposition of metal oxides on pristine and functionalized graphene. *J Am Chem Soc*. 2008;130(26):8152–8153.
22. Knez M, Kadri A, Wege C, Gösele U, Jeske H, Nielsch K. Atomic layer deposition on biological macromolecules: metal oxide coating of tobacco mosaic virus and ferritin. *Nano Lett*. 2006;6(6):1172–1177.
23. Lee S-M, Pippel E, Gösele U, Dresbach C, Qin Y, Chandran CV, Bräuniger T, Hause G, Knez M. Greatly increased toughness of infiltrated spider silk. *Science*. 2009;324(5926):488–492.
24. McCool BA, DeSisto WJ. Synthesis and characterization of silica membranes prepared by pyridine-catalyzed atomic layer deposition. *Ind Eng Chem Res*. 2004;43(10):2478–2484.
25. McCool BA, DeSisto WJ. Amino-functionalized silica membranes for enhanced carbon dioxide permeation. *Adv Funct Mater*. 2005; 15(10):1635–1640.
26. Alsyouri HM, Langheinrich C, Lin Y, Ye Z, Zhu S. Cyclic CVD modification of straight pore alumina membranes. *Langmuir*. 2003; 19(18):7307–7314.
27. Jiang YB, Xomeritakis G, Chen Z, Dunphy D, Kissel DJ, Cecchi JL, Brinker CJ. Sub-10 nm thick microporous membranes made by plasma-defined atomic layer deposition of a bridged silsesquioxane precursor. *J Am Chem Soc*. 2007;129(50):15446–15447.
28. Liang X, Lu X, Yu M, Cavanagh AS, Gin DL, Weimer AW. Modification of nanoporous supported lyotropic liquid crystal polymer membranes by atomic layer deposition. *J Membr Sci*. 2010;349(1–2):1–5.
29. Nikkola J, Sievanen J, Raulio M, Wei J, Vuorinen J, Tang CY. Surface modification of thin film composite polyamide membrane using atomic layer deposition method. *J Membr Sci*. 2014;450:174–180.
30. Li N, Zhang J, Tian Y, Zhang J, Zhan W, Zhao J, Ding Y, Zuo W. Hydrophilic modification of polyvinylidene fluoride membranes by ZnO atomic layer deposition using nitrogen dioxide/diethylzinc functionalization. *J Membr Sci*. 2016;514:241–249.
31. Alam J, Alhoshan M, Dass LA, Shukla AK, Muthumareeswaran MR, Hussain M, Aldwayyan AS. Atomic layer deposition of TiO_2 film on a polyethersulfone membrane: separation applications. *J Polym Res*. 2016;23(9):183.
32. Shang R, Goulas A, Tang CY, de Frias Serra X, Rietveld LC, Heijman SG. Atmospheric pressure atomic layer deposition for tight ceramic nanofiltration membranes: synthesis and application in water purification. *J Membr Sci*. 2017;528:163–170.
33. Li N, Tian Y, Zhang J, Sun Z, Zhao J, Zhang J, Zuo W. Precisely-controlled modification of PVDF membranes with 3D TiO_2/ZnO nanolayer: enhanced anti-fouling performance by changing hydrophilicity and photocatalysis under visible light irradiation. *J Membr Sci*. 2017;528:359–368.
34. Li F, Li L, Liao X, Wang Y. Precise pore size tuning and surface modifications of polymeric membranes using the atomic layer deposition technique. *J Membr Sci*. 2011;385–386:1–9.
35. Wang Q, Wang X, Wang Z, Huang J, Wang Y. PVDF membranes with simultaneously enhanced permeability and selectivity by breaking the tradeoff effect via atomic layer deposition of TiO_2. *J Membr Sci*. 2013;442:57–64.
36. Xu Q, Yang J, Dai J, Yang Y, Chen X, Wang Y. Hydrophilization of porous polypropylene membranes by atomic layer deposition of TiO_2 for simultaneously improved permeability and selectivity. *J Membr Sci*. 2013;448:215–222.
37. Chen H, Kong L, Wang Y. Enhancing the hydrophilicity and water permeability of polypropylene membranes by nitric acid activation and metal oxide deposition. *J Membr Sci*. 2015;487:109–116.
38. Sheng T, Kong L, Wang Y. Crosslinking of polyimide atomic-layer-deposited on polyethersulfone membranes for synergistically enhanced performances. *J Membr Sci*. 2015;486:161–168.
39. Xiong S, Sheng T, Kong L, Zhong Z, Huang J, Wang Y. Enhanced performances of polypropylene membranes by molecular layer deposition of polyimide. *Chin J Chem Eng*. 2016;24(7):843–849.
40. Wang H, Wei M, Zhong Z, Wang Y. Atomic-layer-deposition-enabled thin-film composite membranes of polyimide supported on nanoporous anodized alumina. *J Membr Sci*. 2017;535:56–62.
41. Chen H, Lin Q, Xu Q, Yang Y, Shao Z, Wang Y. Plasma activation and atomic layer deposition of TiO_2 on polypropylene membranes for improved performances of lithium-ion batteries. *J Membr Sci*. 2014;458:217–224.
42. Xu Q, Yang Y, Wang X, Wang Z, Jin W, Huang J, Wang Y. Atomic layer deposition of alumina on porous polytetrafluoroethylene membranes for enhanced hydrophilicity and separation performances. *J Membr Sci*. 2012;415–416:435–443.
43. Xu Q, Yang Y, Yang J, Wang X, Wang Z, Wang Y. Plasma activation of porous polytetrafluoroethylene membranes for superior hydrophilicity and separation performances via atomic layer deposition of TiO_2. *J Membr Sci*. 2013;443:62–68.
44. Kong L, Wang Q, Xiong S, Wang Y. Turning low-cost filter papers to highly efficient membranes for oil/water separation by atomic-layer-deposition-enabled hydrophobization. *Ind Eng Chem Res*. 2014;53(42):16516–16522.
45. Xiong S, Kong L, Zhong Z, Wang Y. Dye adsorption on zinc oxide nanoparticulates atomic-layer-deposited on polytetrafluoroethylene membranes. *AIChE J*. 2016;62(11):3982–3991.

46. Aarik J, Aidla A, Mändar H, Uustare T, Schuisky M, Hårsta A. Atomic layer growth of epitaxial TiO_2 thin films from $TiCl_4$ and H_2O on α-Al_2O_3 substrates. *J Cryst Growth*. 2002;242(1–2):189–198.
47. Ferguson J, Yoder A, Weimer A, George S. TiO_2 atomic layer deposition on ZrO_2 particles using alternating exposures of $TiCl_4$ and H_2O. *Appl Surf Sci*. 2004;226(4):393–404.
48. Aarik J, Aidla A, Mändar H, Sammelselg V. Anomalous effect of temperature on atomic layer deposition of titanium dioxide. *J Cryst Growth*. 2000;220(4):531–537.
49. Vacassy R, Guizard C, Thoraval V, Cot L. Synthesis and characterization of microporous zirconia powders: application in nanofilters and nanofiltration characteristics. *J Membr Sci*. 1997;132(1):109–118.
50. Puhlfurss P, Voigt A, Weber R, Morbe M. Microporous TiO_2 membranes with a cut off < 500 Da. *J Membr Sci*. 2000;174(1):123–133.
51. Benfer S, Popp U, Richter H, Siewert C, Tomandl G. Development and characterization of ceramic nanofiltration membranes. *Sep Purif Technol*. 2001;22–23(1–2):231–237.
52. Chen X, Zhang W, Lin Y, Cai Y, Qiu M, Fan Y. Preparation of high-flux gamma-alumina nanofiltration membranes by using a modified sol-gel method. *Microporous Mesoporous Mater*. 2015;214:195–203.
53. Sentana I, Puche RD, Sentana E, Prats D. Reduction of chlorination byproducts in surface water using ceramic nanofiltration membranes. *Desalination*. 2011;277(1–3):147–155.
54. Da X, Chen X, Sun B, Wen J, Qiu M, Fan Y. Preparation of zirconia nanofiltration membranes through an aqueous sol-gel process modified by glycerol for the treatment of wastewater with high salinity. *J Membr Sci*. 2016;504:29–39.
55. Van Gestel T, Vandecasteele C, Buekenhoudt A, Dotremont C, Luyten J, Leysen R, Van der Bruggen B, Maes G. Salt retention in nanofiltration with multilayer ceramic TiO_2 membranes. *J Membr Sci*. 2002;209(2):379–389.
56. Ebrahimi M, Willershausen D, Ashaghi KS, Engel L, Placido L, Mund P, Bolduan P, Czermak P. Investigations on the use of different ceramic membranes for efficient oil-field produced water treatment. *Desalination*. 2010;250(3):991–996.
57. Shen L, Cheng C, Yu X, Yang Y, Wang X, Zhu M, Hsiao BS. Low pressure UV-cured CS–PEO–PTEGDMA/PAN thin film nanofibrous composite nanofiltration membranes for anionic dye separation. *J Mater Chem A*. 2016;4(40):15575–15588.
58. Granneman E, Fischer P, Pierreux D, Terhorst H, Zagwijn P. Batch ALD:Characteristics, comparison with single wafer ALD, and examples. *Surf Coat Technol*. 2007;201:8899–8907.
59. Hirvikorpi T, Laine R, Vähä-Nissi M, Kilpi V, Salo E, Li WM, Harlin A. Barrier properties of plastic films coated with an Al_2O_3 layer by roll-to-toll atomic layer deposition. *Thin Solid Films*. 2014; 550:164–169.

Manuscript received June 22, 2017, and revision received Dec. 21, 2017.